ARTICLE INFO

Article history:
Received 28 August 2013
Received in revised form 18 October 2013
Accepted 3 November 2013
Available online 1 December 2013

Keywords:
Parabolic trough solar collector
Wind loads
Windbreaks
Wind tunnel
Solar power plant

ABSTRACT

Parabolic reflectors, also known as parabolic troughs, are widely used in solar thermal power plants. This kind of power plants is usually located on desert climates, where the combined action of wind and dust can be of paramount importance. In some cases it becomes necessary to protect these devices from the joined wind and sand action, which is normally accomplished through solid windbreaks. In this paper the results of a wind tunnel test campaign, of a scale parabolic trough row having different windward windbreaks, are reported. The windbreaks herein considered consist of a solid wall with an upper porous fence. Different geometrical configurations, varying the solid wall height and the separation between the parabolic trough row and the windbreak have been considered. From the measured time series, both the mean and peak values of the aerodynamic loads were determined. As it would be expected, mean aerodynamic drag, as well as peak values, decrease as the distance between the windbreak and the parabolic increases, and after a threshold value, such drag loads increase with the distance.

1. Introduction

One of the most promising options to substitute the increasing demand of conventional energy is the solar thermal power plant. The collected solar energy can be used either to generate electricity or to water desalination, amongst other related applications. Converting solar energy into electricity can be performed by converting the direct radiation to thermal energy by means of solar collectors or concentrators, carried by working fluid to a conventional process of electricity generation. In this case, parabolic reflectors in a trough configuration are normally used. Parabolic troughs collectors (PTC) are the most proven and mature solar thermal technology, giving rise to parabolic-trough power plants (or solar farm). A solar farm is composed of a large field of PTC, a heat exchanger block and a conventional turbine-generator system. Solar fields comprise rows of PTC aligned north-south which can track sun direct radiation during the day.

Since the beginning of its commercial use in the eighties (between 1984 and 1991 nine power plants with an overall capacity of 354 MW have been installed in the Mojave Desert in California), a renewed interest in concentrating solar power has rapidly grown worldwide. A complete overview of the parabolic-trough collectors that have been built and marketed during the last decades, the prototypes currently under development, and a survey of systems which could incorporate this type of concentrating solar system for electricity generation can be found in Kalogirou [1], Fernández-García et al. [2] and in Siva Reddy et al. [3].

Siva Reddy et al. [3] and Timilsina et al. [4] agree in that, despite the intense development of this technology, even today the cost per kW of solar power is higher and the overall efficiency of the system is lower. Nevertheless, they show that the cost of solar power may become competitive very soon. As stated in Geyer et al. [5], one of the cost reductions potential is the simplification of the design, which includes the optimization of the structure. Due to the typical location of the solar farms and its geometrical features, they are subject to high loads caused by the wind. So, to achieve this optimization it is necessary to reduce uncertainty in

the knowledge of the wind loads over the PTCs and seek methods of reducing them (among other things, of course). But, as Zemler et al. [6] mentioned, there are very little reliable work done to investigate the forces of the wind on parabolic solar collectors. Studies concerning wind effects on full scale solar troughs are scarce and limited [7], although some attempts have been made to study wind loads on solar collectors by means of wind tunnel testing like Lüpfert et al. [8], Hosoya et al. [9] and Rheem et al. [10], or by numerical simulations, like Naeeni and Yaghoub [11], Christo [12], Hachicha et al. [13] and Zemler et al. [6].

Wind tunnel measurements show that the solar collector field of a full size plant could be divided into three different wind loading zones: the wind-shadowed inner field area with approximately 95% of the total solar collector elements, the transient area (close to the edges of the field) with about 2.5% and the high wind loaded edges and rim areas where about 2.5% of the total solar collectors are located [8].

On the other hand, since parabolic-trough collectors are based on the concentration of the solar radiation to achieve high temperatures necessary for the thermo-dynamic power plant process, their application areas are restricted to Earth regions with high direct solar radiation. Initiatives dealing with large solar collector plants in countries all along this sunny belt have been reported: Mediterranean countries [14,15], Alger [16], Tunisia [17], Jordan [18], Arabia [19], Iran [20] and Pakistan [21], among others. Arab countries also belong to such regions and represent therefore potential areas for the application of solar energy for electricity generation [22]. Therefore, the most suitable locations seem to be the desert-like regions close to the Earth equator and other neighboring regions. This implies that solar farms are additionally exposed to large amounts of dust, which affects the efficiency and deteriorates the mechanisms, among other problems. Sarver et al. [23] provides a comprehensive overview of problems associated with dust conditions that are inherent to the mentioned regions.

For security reasons, parabolic-trough solar plants are usually enclosed with fences made of wire mesh. In most cases a standard grid fence is enough to meet all the protection and operational requirements; and they perform a function of windproof barrier and dust protection as well. Moreover, mainly in sandy places like deserts, the grid fences are substituted by a solid wall with a porous fence on its top.

The aerodynamic action of a fence is explained by considering that a fence exerts a drag force on the wind field, causing a net loss of momentum in the air flow, thus creating a sheltering effect. In the case of low porosity fences (porosity, ϕ, is the ratio of the frontal open area of porous fence to the frontal area of fence, so that $\phi = 0$ means a solid wall), a large region of separated flow in the lee of the fence is created, provided the porosity is below a certain value. For a solid fence this separation region can be approximated to a triangular zone extending from the top of the fence, whose height is h, to the ground at a distance around 7.5 times the fence height, depending on the turbulence intensity [24,25]. The more solid the fence, the stronger is the turbulence in the separation bubble and the steeper the return of the displacement flow to the ground at its downstream reattachment point. As porosity increases, the separation bubble diminishes in size and moves downstream. The separation bubble disappears at $\phi \cong 0.35$. The type of porosity has an effect only in the very near wake, less than 2.5 times the fence height (g). The influence of porosity in the far wake is negligible even for low porosity fences.

Aiming to get some insight on the aerodynamic interaction between the fence and the parabolic trough, a set of wind tunnel experiments has been performed. Wind loads on a model of standard parabolic trough have been measured under different upstream conditions. The height of the solid wall (*SW*), the height of the porous fence (*PW*) placed on top of the solid wall and the distance between the fence and the PTC (d), have been modified in order to obtain different configurations (Fig. 1). Since real parabolic troughs are immersed in the atmospheric boundary layer, where the incident flow is non-uniform and highly turbulent, wind actions on the solar collectors are time dependent. Therefore, the aerodynamic tests have been performed in a wind tunnel where the atmospheric boundary layer can be simulated.

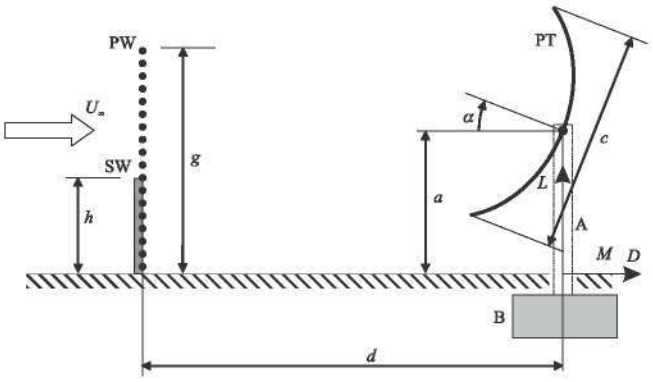

Fig. 1. Sketch of the model for wind tunnel measurements. PT) parabolic trough, (A) supporting arms, (B) six-axes balance, (PW) porous fence, (SW) solid wall. The nomenclature used to define this configuration is: parabolic trough chord, c, height of the solar collector axis, a, distance from the parabolic trough axis to the windbreak, d, height of the solid part of the windbreak, h, height of the porous part of the windbreak, g, angle of attack, α.

In the following section the experimental setup and procedures are described. Experimental results are presented in Section 3, and the conclusions are outlined in Section 4.

2. Experimental setup and procedures

Experiments were performed at the ACLA16 atmospheric boundary-layer wind tunnel of IDR/UPM. This is a low-speed closed return wind tunnel with a closed test section, which has a squared cross section with 2.2 m side length and 17 m length (Fig. 2). The wind tunnel is driven with 16 fans, 7.5 kW each one (the total power is 120 kW). The wind speed is controlled electronically by means of a variable frequency drive, and flow velocities up to 30 m/s can be attained.

To reproduce the appropriate scaled turbulent boundary layer, part of the test section is covered with suitable roughness elements. The resulting boundary layer simulates approximately an open terrain type as defined in ASCE 7-05 [26]; in which the variation of wind speed, U, with the height over the terrain, z, is represented by the power law $U(z) \propto U_{10}(z/z_{10})^{\alpha}$, where U_{10} is the mean velocity at $z_{10} = 10$ m, and $\alpha = 2/13$. The longitudinal turbulence intensity is defined as $I_u(z) \propto (z_{10}/z)^b$, with $b = 1/6$. The variation of both, the time-averaged velocity and the turbulence intensity, with the distance to the ground is represented in Fig. 4. In the same plot, the values as given by the ASCE 7-05 [26] boundary layer model are plotted with solid lines. Moreover, Fig. 5 shows the reduced power spectral density (PSD) of turbulent fluctuations as a function of Monin coordinate, determined at the height which corresponds to z_{10}. Also, the Kaimal's model of PSD is plotted in the same figure. It can be concluded that the flow in the test chamber reproduces satisfactorily the inertial sub-range atmospheric turbulent fluctuations. This wind profiles were measured with a hot-wire anemometry equipment (Dantec Dynamics CTA 90C10 and a 55p16 probe) and a linear stage. For each z coordinate, measurements were carried out at a rate of 2 kHz during a sampling time of 120 s.

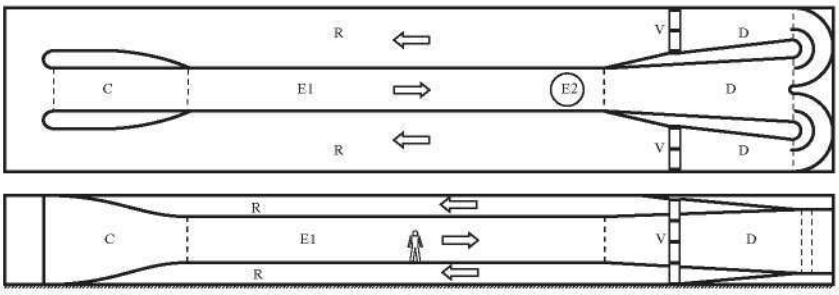

Fig. 2. ACLA16 boundary layer wind tunnel top and front views. E1 and E2, test section; R, return circuit; V, fans; D, diffuser; and C, contraction.

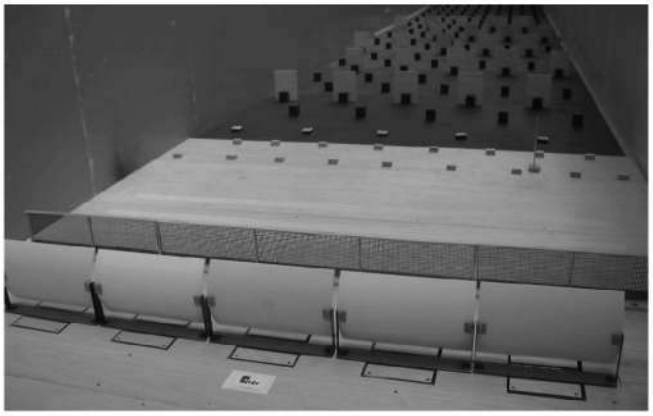

Fig. 3. Parabolic trough and windbreak models used in the experimental campaign. Roughness elements placed upstream of the model are used to generate the atmospheric boundary layer.

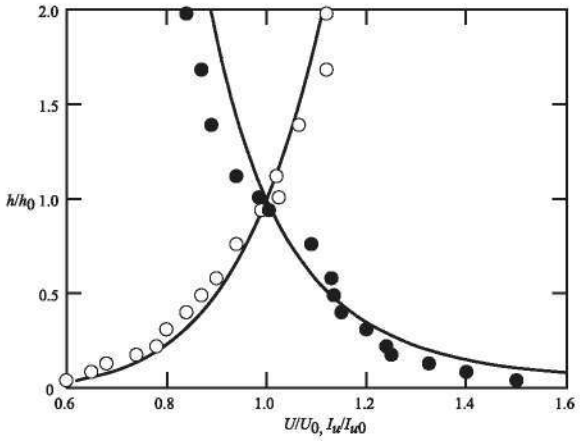

Fig. 4. Variation with the dimensionless height over the terrain, h/h_0, of the dimensionless mean wind velocity profile, U/U_0 (open circles) and the dimensionless turbulent intensity profile, I_u/I_{u0} (closed circles) measured in the ACLA16 wind tunnel. The subscript 0 indicates reference values at 10 m height at real scale. Theoretical profiles corresponding to open terrain as given in ASCE 7-05 [26] are also shown (solid lines).

The test model consists of a row of collectors with five parabolic trough modules placed downstream the roughness elements, as shown in Fig. 3. The geometrical scale is 1/45. This scale has been selected looking for a good relation between the size of the model and the blockage in the test chamber. Each model consist of a parabolic trough, made with a 3D printer (stereo-lithographic technique), and two supporting arms. The thickness of the supporting arms is around 1 mm. Each parabolic trough is anchored to the arms by its rotating axis by a very simple mechanism, which allows the rotation of the parabola at any angle of attack. Supporting arms are fixed to a base plate made of aluminum, which in turn is fixed to a 6-axes load cell (AMTi instruments, model HE6×610) located just below the wind tunnel floor (actually, the whole experimental setup is mounted on a vertical wall of the ACLA16 wind tunnel, to facilitate its handling and manipulation). The upper surface of the base plate is at the same level than the surrounding floor, $z = 0$. As can be seen in Fig. 3, five load cells were used, so that wind loads on the five trough models of a row were measured simultaneously. The weight of the whole model (parabola, arms and base plate) is low enough to avoid inertial effects during wind load measurements and its first natural frequency is larger than 42 Hz. Since the aim of this work is to evaluate the effects of upstream wind barriers on the aerodynamic loads acting on the first row of a solar plant model, only one row of troughs has been considered, as well as only one value of the yaw angle (the wind is perpendicular to the row of troughs) and one value of pitch angle, $\alpha = 0°$. Roughly speaking, that configuration corresponds to critical conditions in which the maximum drag is reached. Testing of others configurations are left for future works.

It must be stressed that the measured wind loads include not only the effects on the parabolic surface, but also the effects on the supporting arms. However due to the small area exposed to the wind, their contribution to the total measured loads is small compared to the loads acting on the parabolic surface. Roughly speaking, the ratio of these loads is proportional to the ratio of wind exposed areas, which is less than 0.003.

Several types of windbreaks have been considered. As sketched in Fig. 1, a typical windbreak consists of a solid wall placed at the

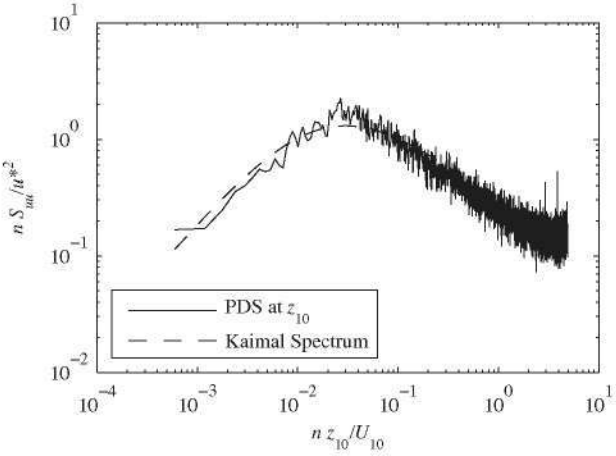

Fig. 5. Reduced power spectral density of turbulent fluctuations as a function of Monin coordinate, determined at the height corresponding to z_{10} (continuous line). The Kaimal's model of PSD in dashed line.

windward side of the wind barrier and a porous fence placed just behind, in the leeward side. Solid walls are made of wood, with heights varying from 0% of the parabola's chord, c, to 60% of c at 20% steps. Porous fences are made of a commercial plastic mesh with 50% porosity, two heights have been considered, namely 56% and 80% c. With this configuration the porous fence can be more or less covered by the solid wall. The values of the different geometrical parameters are summarized in Table 1. In this table all lengths are made dimensionless by using the parabola's chord as characteristic length. In addition to the different windbreaks configurations, several distances from the wind barrier to the parabolic trough row were tested; these distances were $d = n \cdot c$, where $n = 1, 2, \ldots 7$. Note that a clean configuration (without any wind barrier) has been measured, as well.

A Pitot static tube has been placed at the end of the roughness elements zone at a height of 222 mm over the model floor, which corresponds to a height of 10 m at full scale. In order to determine the reference dynamic pressure, the Pitot tube has been connected to a Druck LPM9381 differential pressure transducer. The instrumentation is completed with a computer and a 16 bit A/D board from National Instruments (model Compact DAQ System NI 9205), which acquired the analog outputs of the load cells and the pressure transducer. Measurements were recorded at a sampling rate of 200 Hz during 236 s. The sampling rate was selected taking into account the expected frequency of vortex shedding at the maximum wind tunnel speed (about 10 Hz), and the sample period has been determined considering the time scale of the test, and to have at least, an equivalent period of 40 min at full scale.

Even in the worst case the blockage ratio of the model section to the working cross-section of the test chamber was smaller than 0.06 (considering either the parabolic trough or the wind barriers), so that no provisions for blockage correction were undertaken. The Reynolds number based on parabola's chord, c, was about 2.5×10^5. According to Larose and D'Auteuil [27], this Reynolds number is the best trade-off to fulfill blockage corrections and to avoid results dependency on Reynolds number.

In a real solar-trough farm, since the design criteria is to avoid the shadowing of the different parabolic mirrors during the sunny hours, the distance between rows is driven by the local latitude. According to this criterion, a typical separation between rows is about $d \cong 3c$, and the distance between external rows and perimeter fences should be similar. In wind tunnel tests, as already stated, the distance from the perimeter to the first row has been varied in the range $1 \leqslant d/c \leqslant 7$.

3. Results and discussion

Experimental measurements have been analyzed by following the standard procedures used when wind loads measured in wind tunnels with simulated atmospheric boundary layer are considered [26]. Since the uncertainty is inversely proportional to the root square of the number of samples ($N = 4.72 \times 10^4$), this criterion applies for the reported mean values of the aerodynamic loads, whereas the uncertainty of the instrumentation is an upper limit for the uncertainty of peak loads.The experiment outputs were the time series of the dynamic pressure in the wind tunnel test chamber, $q_\infty(t) = \rho U_\infty^2(t)/2$, and the six components of the aerodynamic loads. Although in the following only the drag force, $D(t)$, the lift force, $L(t)$ and the pitching moment at the parabola foundations, $M(t)$, are considered. From these magnitudes, the aerodynamic drag coefficient, $c_D(t) = D(t)/(q_\infty(t) \cdot S)$, lift coefficient, $c_L(t) = L(t)/(q_\infty(t) \cdot S)$, and the pitching moment coefficient, $c_M(t) = M(t)/(q_\infty(t) \cdot S \cdot c)$, were determined. In the above expressions, S the frontal area of the parabolic trough, $S = c \cdot b$, where b is trough's width a c its chord (see Fig. 1).

Although wind loads were measured in the five solar trough models forming the test row, in the following only results corresponding to the central module are considered. It had been observed that the results for the three central modules are almost the same, independently of their position within the row. This means that such modules behave as a two-dimensional configuration.

The aerodynamic coefficients determined in the reference configuration (without any wind barrier, configuration 00-00 in Table 1) are presented in Table 2. These results are in concordance with the ones obtained by Christo [12] and Hosoya et al. [9] for similar configurations.

In order to appreciate the effects of the wind barriers on the aerodynamics loads, Figs. 6 and 7 show the variation of the reduced mean load coefficients and the corresponding reduced standard deviations with the dimensionless distance, d/c. That means that every mean coefficient was divided by the corresponding values obtained without any windbreak in front of the solar collectors (configuration 00-00 in Table 1).

In Fig. 6 it can be observed the influence on the aerodynamics loads of a solid wall alone (configuration 60-00), a porous windbreak alone (configuration 00-80), and the combination of the two previous windbreaks (configuration 60-80). Also, the results for different heights of the solid wall for the same porous windbreaks are presented. Fig. 7 shows similar plots but for $g/c = 56\%$.

It can be observed that all the windbreak configurations significantly reduce the mean values of the aerodynamics forces and moment, and that the effect of load reduction is lost as the distance between the fences and the parabolic troughs increases. It could be expected that, at some distance greater than 7 d/c, the effect of the wind barriers completely disappears. At $d/c = 1$ the decrease of the mean load is somewhat lower. In fact, for some configurations the reduced lift coefficient becomes greater than one. So, when the fences are at dimensionless distances d/c between 2 and 4, the mean loads are minimum. This behavior is similar for any wind barrier configuration. This effect is due to the complex interaction between the wake of the windproof barrier and parabolic collector. When walls are located close enough to the trough, either with or without meshes on the top, it reduces the flow velocity at the bottom part of the parabola and increases it at the top.

Table 1
Values of the dimensionless parameters defining the test configurations: h, g, and d, where h is the solid wall height, g the height of the porous fence placed behind the solid wall, and d the horizontal distance from the windbreak to the axis of the parabolic trough, expressed as percent of the solar collector chord, c. In the table the first two digits gives $100 \cdot h/c$, whereas the second group of two digits represents $100 \cdot g/c$. The distance between the parabolic row and windbreak is $d = n \cdot c$, with $n = 1,2,3,\ldots 7$. The configuration 00-00 corresponds to a solar trough without any upstream windbreak.

	h/c			
	00%	20%	40%	60%
g/c				
00%	00-00			60-00
56%	00-56	20-56	40-56	
80%	00-80	20-80	40-80	60-80

Table 2
Mean aerodynamic load coefficients and its corresponding measured standard deviation for the 00-00 configuration (see Table 1).

	Mean value	Standard deviation
c_D	1.43	0.202
c_L	0.14	0.036
c_M	0.70	0.102

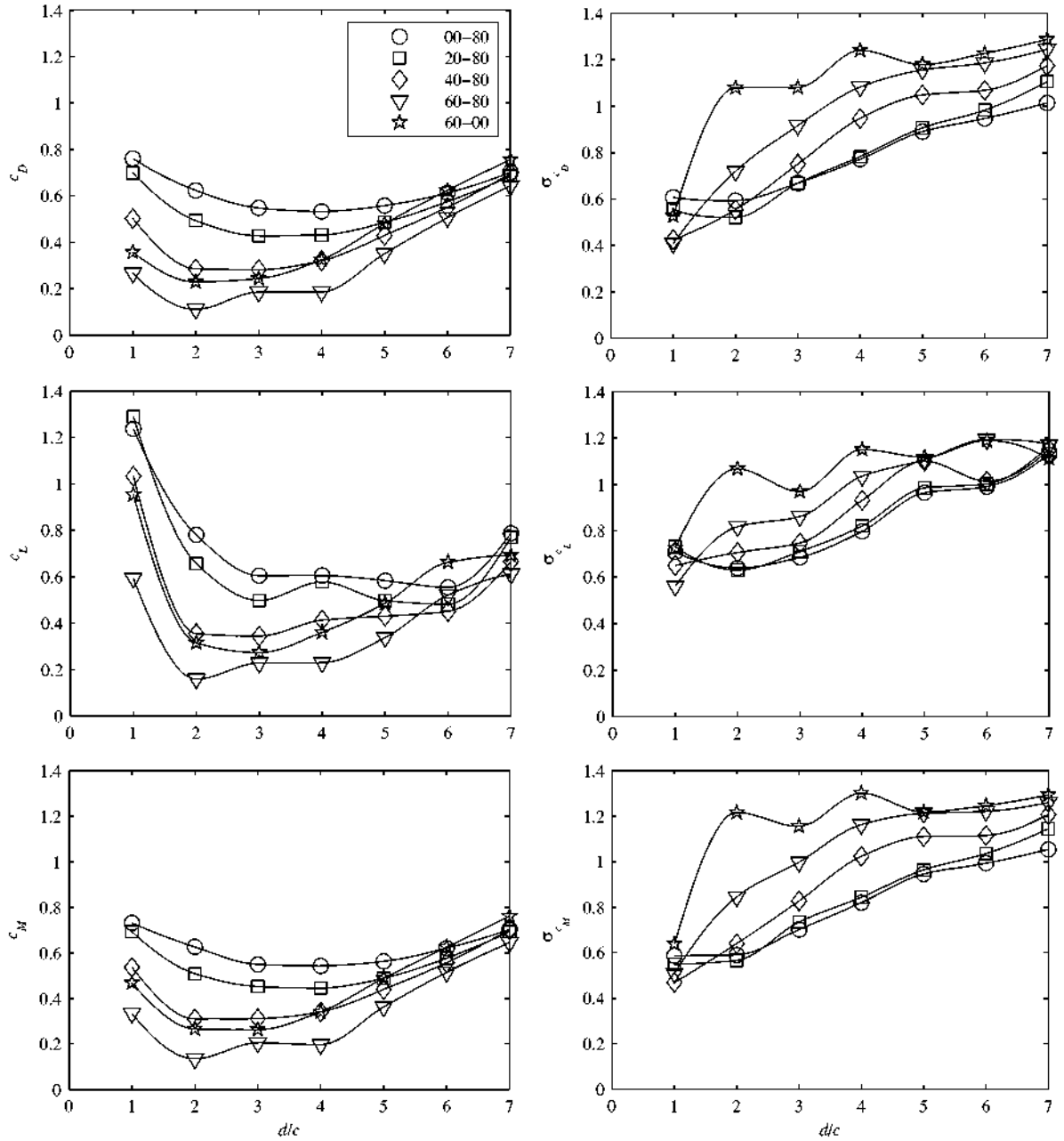

Fig. 6. On the left column, variation of the mean aerodynamic load coefficients (c_D, c_L and c_M) with the dimensionless distance, d/c. On the right column, the corresponding standard deviation of the measured time series. Symbols identify the windbreak configurations.

Regarding the standard deviation, note that in all cases it increases as d/c does and, for certain configurations, it becomes even larger than the value corresponding to a trough without wind barriers. In this sense, the worst case corresponds to the solid wall alone (configuration 60-00) and the best one corresponds to the porous windbreak alone (configuration 00-80). Such behavior is a consequence of the interaction between the turbulent wake (caused by the solid wall) and the parabolic trough. When grids are added on top of the walls, the shear layer detached at the top of the walls is smoothened. The grid diminishes the turbulence intensity past the wall and, consequently, standard deviation values also diminish. The smaller the solid wall, the smaller the recirculation bubble and the effects of the turbulence are mitigating by the porous fence, resulting in smaller standard deviations. When the size of the solid wall is increased, the recirculation bubble size increases, its effects is not totally mitigated by the porous fence and the turbulence generated by the shear layer is reflected in the standard deviations.

From the design point of view, the increase of the standard deviations of the loads is an undesired effect, because it could result in greater load peak values. Also, greater standard deviations imply that the aerodynamic loads have greater amplitude fluctuations, which is not desirable from the standpoint of fatigue phenomena.

The peak load values for Gaussian process can be determined as the mean values plus the standard deviation multiplied by the peak factor, k, that is: $c_{D\,\mathrm{peak}} = c_D + k \cdot \sigma_{cD}$, $c_{L\,\mathrm{peak}} = c_L + k \cdot \sigma_{cL}$, $c_{M\,\mathrm{peak}} = c_M + k \cdot \sigma_{cM}$; where k depends on the natural frequency of the structure and the considered time interval [28,29]. Fig. 8 shows the peak load values obtained in this way, considering a peak factor

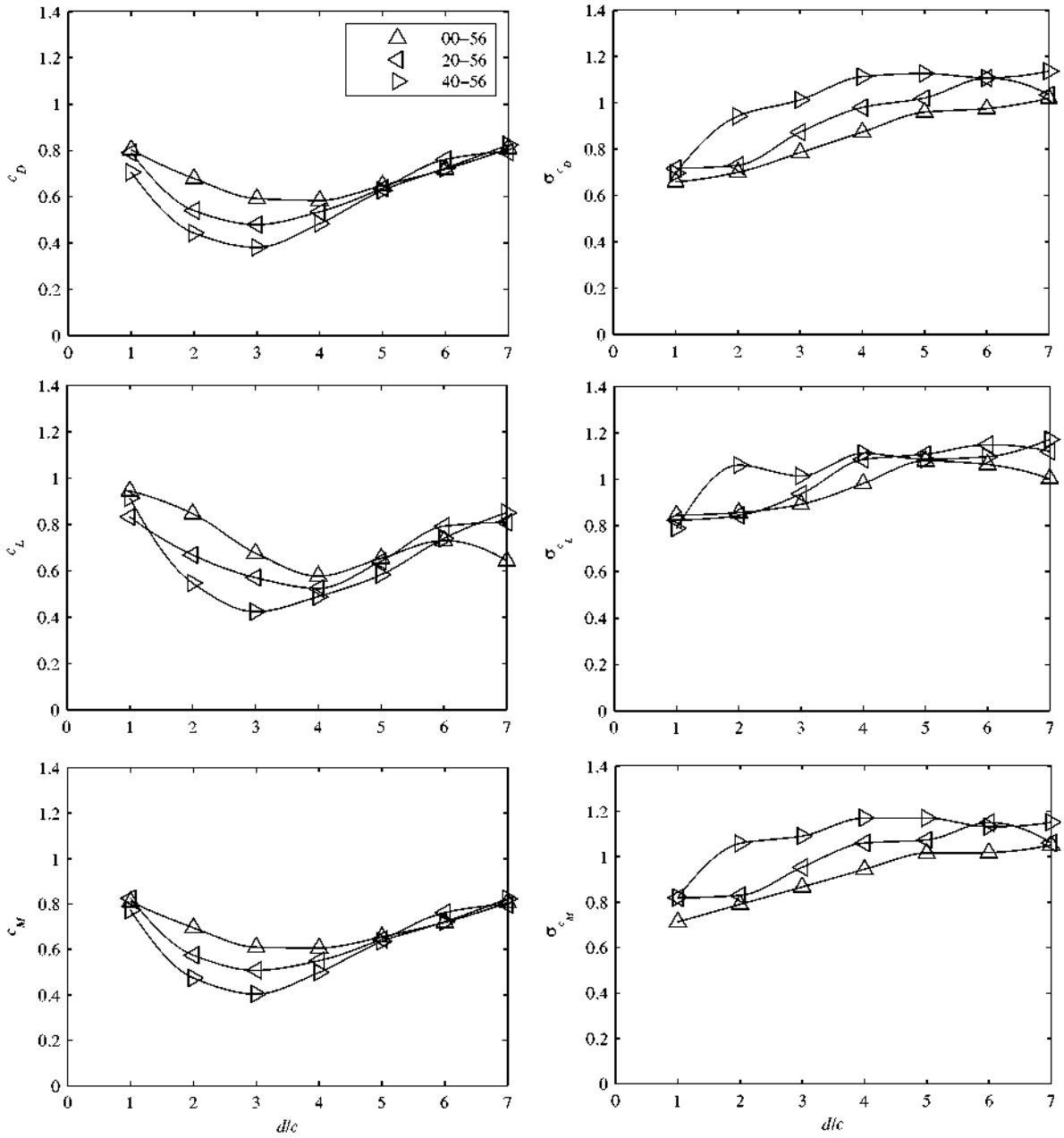

Fig. 7. On the left column, variation of the mean aerodynamic load coefficients (c_D, c_L and c_M) with the dimensionless distance, d/c. On the right column, the corresponding standard deviation of the measured time series. Symbols identify the windbreak configurations.

$k = 3.5$, just for configurations 00-80, 60-00 and 60-80. The peak load coefficient curves present a minimum at distances between $d/c \cong 1$ and $d/c \cong 3$, this behavior being almost the same independently of the wind barrier configuration, but the most efficient is the configuration 60-80. So, it can be concluded that it is possible to reduce the wind loads over the front row of a parabolic troughs plant up to 60%, with an adequate selection of windbreaks configuration.

Summarizing, the flow past a windbreak is driven by boundary layer separation at the windbreak, provided its porosity is low enough. In the case of a solid wall, boundary layer separates at the upper windward edge of the windbreak and the resulting shear layer reattaches at a given distance, forming a recirculation bubble downstream the wall. On the other hand, if the porosity is high enough the recirculation bubble is swept downstream and the reattachment phenomenon does not occur. In the former case a wide wake downstream the windbreak is formed due to boundary layer separation, the height of the separation point over the floor increasing as the parapet height increases, and the vertical distance of the shear layer to the floor increases accordingly. For some values of the parameters g/c, h/c and d/c the resulting shear layer reach the parabolic trough, therefore increasing the turbulence intensity at the parabolic mirror, and thus the peak aerodynamic loads. In a solid wall with a grid fence on its top, since the intensity of the wind velocity over the recirculation bubble is decreased because of the porous grid, it could expect a smoothened shear layer, thence a decrease of the turbulence intensity of such shear layer when impinges on the solar collector.

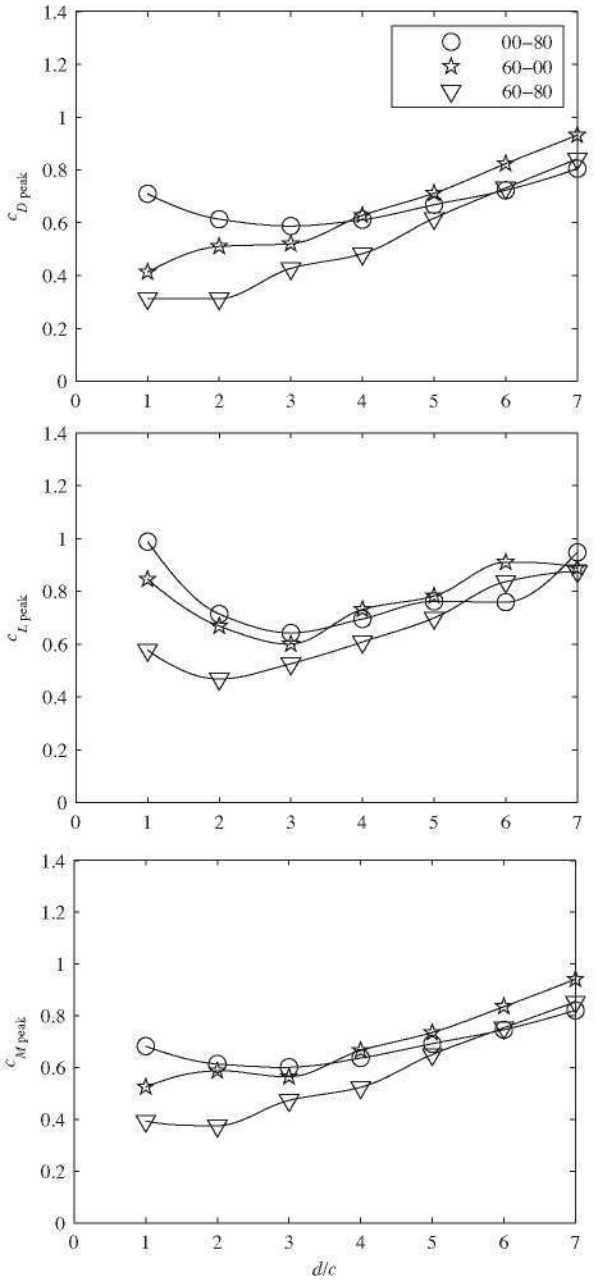

Fig. 8. Variation of the peak aerodynamic loads (c_D, c_L and c_M) with the dimensionless distance, d/c.

4. Conclusions and future works

In sandy areas, the use of windbreaks consisting of a solid wall with a porous fence on top of the solid wall is recommended because these configurations protect the mirrors against the dust and facilitates the removal of accumulated sand in the windward of the barrier. The influence of this kind of windbreaks on the aerodynamic loads acting on the solar troughs closest to the windbreak has been analyzed through wind tunnel tests.

As it is expected, any configuration of wind barrier reduces the mean aerodynamics loads over the PTCs. However, with the appropriate selection the parameters g/c, h/c and d/c it is possible to reduce the aerodynamics loads (mean and peaks values) up to 60% over the first row of PTCs (which are the most loaded ones [8]).

Under these conditions it is possible to design an optimized PTC's supporting structure, and therefore, advance in the searched cost reduction. Nevertheless, for some configurations and distances $d/c > 5$, the shear layer produced by the windbreak reaches the parabolic trough, resulting in higher peak values of the aerodynamic loads.

Nowadays, additional wind tunnel tests are running with the aim to evaluate the effect of these particular windbreaks on the following rows and for different angles of incidence of the wind and different angles of attack of the PTC.

Acknowledgement

This work has been partially supported by the *Consejo Nacional de Ciencia y Tecnología* (*México*) through its scholarships program, which the first author is recipient.

References

[1] Kalogirou SA. Solar thermal collectors and applications. Prog Energy Combust Sci 2004;30:231–95.
[2] Fernández-García A, Zarza E, Valenzuela L, Pérez M. Parabolic-trough solar collectors and their applications. Renew Sust Energy Rev 2010;14:1695–721.
[3] Siva Reddy V, Kaushik SC, Ranjan KR, Tyagi SK. State-of-the-art of solar thermal power plants – a review. Renew Sust Energy Rev 2013;27:258–73.
[4] Timilsina GR, Kurdgelashvili L, Narbel PA. Solar energy: markets, economics and policies. Renew Sust Energy Rev 2012;16:449–65.
[5] Geyer M, Lüpfert E, Osuna R, Esteban A, Schiel W, Schweitzer A, et al. EuroTrough – parabolic trough collector developed for cost efficient solar power generation. In: Proceedings of the 11th Int. symposium on concentrating solar power and chemical energy technologies; 2002 September 4–6; Zurich, Switzerland.
[6] Zemler MK, Bohl G, Rios O, Boetcher SKS. Numerical study of wind forces on parabolic solar collectors. Renew Energy 2013;60:498–505.
[7] Gong B, Wang Z, Li Z, Zhang J, Fu X. Field measurements of boundary layer wind characteristics and wind loads of a parabolic trough solar collector. Sol Energy 2012;86:1880–98.
[8] Lüpfert E, Geyer M, Schiel W, Esteban A, Osuna R, Zarza E, et al. EuroTrough design issues and prototype testing at PSA. In: Proceedings of solar forum 2001 solar energy: the power to choose; 2001 April 21–25; Washington DC, USA.
[9] Hosoya N, Peterka JA, Gee R, Kearney D. Wind tunnel tests of parabolic trough solar collectors. Tech. rep. NREL/SR-550-32282, National Renewable Energy Laboratory; 2008.
[10] Rheem J, Nguyen C, Grace M, Thu A. An effective, low-cost mechanism for direct drag force measurement on solar concentrators. J Wind Eng Ind Aerodyn 2011;99:665–9.
[11] Naeeni N, Yaghoubi M. Analysis of wind flow around a parabolic collector (1) fluid flow. Renew Energy 2007;32:1898–916.
[12] Christo FC. Numerical modelling of wind and dust patterns around a full-scale paraboloidal solar dish. Renew Energy 2012;39:356–66.
[13] Hachicha AA, Rodríguez I, Castro J, Oliva A. Numerical simulation of wind flow around a parabolic trough solar collector. Appl Energy 2013;107:426–37.
[14] Falchetta M, Manfredi C. Perspectives for concentrating solar power in coastal areas of Mediterranean sea. In: Proceedings of the 5th European seminar "offshore wind and other marine renewable energies in mediterranean and european seas"; 2006 April 20–22; Civitavecchia, Rome, Italy.
[15] Poullikkas A. Economic analysis of power generation from parabolic trough solar thermal plants for the Mediterranean region – a case study for the island of Cyprus. Renew Sust Energy Rev 2009;13:2474–84.
[16] Zaaraoui A, Yousfi ML, Said N. Technical and economical performance of parabolic trough collector power plant under Algerian climate. Procedia Eng 2012;33:78–91.
[17] Balghouthi M, Chahbani MH, Guizani A. Investigation of a solar cooling installation in Tunisia. Appl Energy 2012;98:138–48.
[18] Badran O, Eck M. The application of parabolic trough technology under Jordanian climate. Renew Energy 2006;31:791–802.
[19] Hepbasli A, Alsuhaibani Z. A key review on present status and future directions of solar energy studies and applications in Saudi Arabia. Renew Sust Energy Rev 2011;15:5021–50.
[20] Azizian K, Yaghoubi M, Hesami R, Mirhadi S. Shiraz pilot solar thermal power plant design, construction, installation and commissioning procedure. In: Proceedings of the 7th international conference on heat transfer, fluid mechanics and thermodynamics; 2010 July 19–21; Antalya, Turkey.
[21] Raja NK, Khalil MS, Masood SA, Shaheen M. Design and manufacturing of parabolic trough solar collector system for a developing country Pakistan. J Am Sci 2011;7(1):365–72.
[22] Al-Sakaf OH. Application possibilities of solar thermal power plants in Arab countries. Renew Energy 1998;14:1–9.
[23] Sarver T, Al-Qaraghuli A, Kazmerski LL. A comprehensive review of the impact of dust on the use of solar energy: history, investigations, results, literature, and mitigation approaches. Renew Sust Energy Rev 2013;22:698–733.

[24] ESDU 97031. Estimation of Shelter Provided by Solid and Porous Fences. Engineering Sciences Data Unit 2009, UK.
[25] Nelmes S, Belcher RE, Wood CJ. A method for routine characterization of shelterbelts. Agric For Meteorol 2001;106:303–15.
[26] Minimum Design Loads for Buildings and Other Structures, ASCE/SEI 7-05, Chapter 6, Wind Loads. American Society of Civil Engineers, Reston, USA; 2005.
[27] Larose GL, D'Auteuil A. On the Reynolds number sensitivity of the aerodynamics of bluff bodies with sharp edges. J Wind Eng Ind Aerodyn 2006;94:365–76.
[28] Dyrbye C, Hansen SO. Wind Loads on Structures. John Wiley & Sons; 1996.
[29] Cartwright DE, Longuet-Higgins MS. The statistical distribution of the maxima of a random function. Proc Roy Soc Lond A 1956;237(1209):212–32.